A Control-oriented, Physics-based Model for Ionic Polymer-Metal Composite Actuators

Zheng Chen and Xiaobo Tan

***Abstract*— Ionic polymer-metal composites (IPMCs) form an important category of electroactive polymers (also known as artificial muscles) and have built-in actuation and sensing capabilities. A dynamic, physics-based model is presented for IPMC actuators, which is amenable to model reduction and control design. This model is represented as an infinite-dimensional transfer function relating the bending displacement to the applied voltage. It is obtained by deriving the exact solution to the governing partial differential equation (PDE) in the Laplace domain for the actuation dynamics, where the effects of the distributed surface resistance and the dynamics of the cantilever beam are incorporated. The physical model is expressed in terms of fundamental material parameters and actuator dimensions, and is thus geometrically scalable. It can be easily reduced to low-order models for real-time control design. As an example, an H_∞ controller is designed based on the reduced model and applied to tracking control. Experimental results are provided to validate the proposed model.**

I. INTRODUCTION

Ionic polymer-metal composites (IPMCs) form an important category of electroactive polymers (also known as artificial muscles) and have built-in actuation and sensing capabilities [1]. An IPMC sample typically consists of a thin ion-exchange membrane (e.g., Nafion), chemically plated on both surfaces with a noble metal as electrode [2]. When a voltage is applied across an IPMC, transport of hydrated cations and water molecules within the membrane and the associated electrostatic interactions lead to bending motions, and hence the actuation effect. Fig. 1 illustrates the mechanism of the IPMC actuation. Because of their softness, resilience, biocompatibility and the capability of producing large deformation under a low action voltage, IPMCs are very attractive materials for many applications in the fields of biomedical devices and biomimetic robots [3], [4].

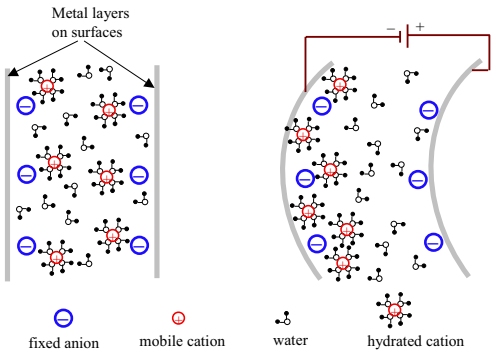

Fig. 1. Mechanism of the IPMC actuation [1].

Z. Chen and X. Tan are with Department of Electrical & Computer Engineering Michigan State University, East Lansing, MI 48824, USA, emails: chenzhe1@egr.msu.edu, xbtan@egr.msu.edu

A faithful and practical model is desirable in real-time control of these novel materials in various potential applications. Current modeling work can be classified into three categories based on their complexity levels. Based purely on the empirical responses, *black-box* models, e.g., [5], offer minimal insight into the governing mechanisms within the IPMC. While these models are simple in nature, they are often sample-dependent and not scalable in dimensions. As a more detailed approach, the *gray-box* models, e.g., [6], are partly based on physical principles while also relying on empirical results to define some of the more complex physical processes. In the most complex form, *white-box* models with partial differential equations (PDEs), e.g., [7], attempt to explain the underlying physics for the sensing and actuation responses of IPMCs, but they are not practical for real-time control purposes. Farinholt derived the impedance response for a cantilevered IPMC beam under step and harmonic voltage excitations [8]. The derivation was based on a linear, one-dimensional PDE governing the internal charge dynamics, which was first developed by Nemat-Nasser and Li for studying the actuation response of IPMCs [7]. While the work of Farinholt [8] is an important progress, it can not be used for model-based controller design.

In this paper, an explicit control-oriented yet physics-based actuation model for IPMC actuators is presented. The model combines the seemingly incompatible advantages of both the white-box models (capturing key physics) and the black-box models (amenable to control design). The proposed modeling approach provides an interpretation of the sophisticated physical processes involved in IPMC actuation from a systems perspective. The starting point of the model development is the same governing PDE as in [7], [8] that describes the charge redistribution dynamics under external electrical field, electrostatic interactions, ionic diffusion, and ionic migration along the thickness direction. As the first step, the impedance model is also derived in order to better understand the ion movement in the IPMC. But this work extends previous studies significantly in three aspects.

First, it incorporates the effect of the distributed surface resistance, which is known to influence the actuation and sensing dynamics [9]. The consideration leads to additional dynamics on IPMC surfaces along the length direction. Second, an exact, analytical solution to the PDE is obtained by converting the original time-domain equation to the Laplace-domain version. Third, instead of limiting to step and harmonic responses only, an arbitrary voltage stimulus is allowed, which is of interest for real applications.

The derived model is in the form of an infinite-dimensional

transfer function involving hyperbolic and square-root terms. It is expressed in terms of fundamental physical parameters and actuator dimensions, and is thus geometrically scalable. It can be further reduced to low-order models in the form of rational transfer functions, which are again scalable.

Experiments have been conducted to validate the proposed dynamic model for an IPMC actuator in a cantilever configuration. Good agreement, both in magnitude and in phase, has been achieved between the experimental measurement and the model prediction for periodic voltage inputs from 0.02 Hz to 20 Hz. The results show that considering the surface resistance and the dynamics of cantilever beam leads to more accurate predictions. The geometric scalability of the actuator model has also been confirmed without re-tuning of the identified physical parameters. An example is further provided to illustrate the use of the proposed model for controller development, where an H_∞ controller is designed based upon a reduced model and applied to tracking control.

The remainder of the paper is organized as follows. The governing PDE is reviewed in Section II. In Section III, the impedance model is derived by exactly solving the PDE, considering the effect of surface resistance. In Section IV, the actuation model is further derived from the impedance model. Model reduction is discussed in Section V. Experimental results on model validation are presented in Section VI. Model-based H_∞ controller design and its real-time implementation are reported in Section VII. Finally, concluding remarks are provided in Section VIII.

II. THE GOVERNING PDE

The governing PDE for charge distribution in an IPMC was first presented in [7] and then used by Farinholt and Leo [8] for investigating the actuation and sensing response. Let $\mathbf{D}$, $\mathbf{E}$, ϕ, and ρ denote the electric displacement, the electric field, the electric potential, and the charge density, respectively. The following equations hold:

$$\mathbf{E} = \frac{\mathbf{D}}{\kappa_e} = -\nabla\phi \ , \tag{1}$$

$$\nabla \cdot \mathbf{D} = \rho = F(C^+ - C^-) \ , \tag{2}$$

where κ_e is the effective dielectric constant of the polymer, F is Faraday's constant, and C^+ and C^- are the cation and anion concentrations, respectively. Since the thickness of an IPMC is much smaller than its length or width, one can assume that $\mathbf{D}$ and $\mathbf{E}$ are restricted to the thickness direction (x-direction) only. The PDE for charge density can be derived [10]:

$$\frac{\partial \rho}{\partial t} - d\frac{\partial^2 \rho}{\partial x^2} + \frac{F^2 dC^-}{\kappa_e RT}\left(1 - C^-\Delta V\right)\rho = 0 \ , \tag{3}$$

where d is the ionic diffusivity, R is the gas constant, T is the absolute temperature, and ΔV is the volumetric change. Nemat-Nasser [7] assumed that the induced stress is proportional to the charge density:

$$\sigma = \alpha_0 \rho \ , \tag{4}$$

where α_0 is the coupling constant.

Farinholt [8] investigated the current response of a cantilevered IPMC beam when the base is subject to step and harmonic actuation voltages. A key assumption is that the ion flux at any point on the IPMC electrodes is zero. This assumption, which serves as a boundary condition for (3), leads to

$$\left(\frac{\partial^3 \phi}{\partial x^3} - \frac{F^2 C^-}{\kappa_e RT}\frac{\partial \phi}{\partial x}\right)\Big|_{x=\pm h} = 0 \ , \tag{5}$$

where $\pm h$ represents the beam surfaces.

III. MODEL OF IMPEDANCE RESPONSE

The objective of this paper is to derive an actuation model for IPMC actuators. From (4), one can derive the actuation model based on the charge density distribution. So as the first step, an impedance model relating the charge density distribution to the voltage input is desirable.

Consider Fig. 2, where the beam is clamped at one end ($z = 0$), and is subject to an actuation voltage producing the tip displacement $w(t)$ at the other end ($z = L$) . The neutral axis of the beam is denoted by $x = 0$.

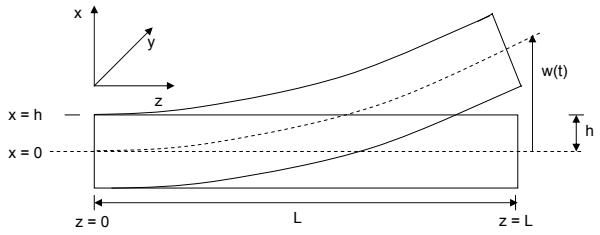

Fig. 2. Geometric definitions of an IPMC beam in the cantilevered configuration (side view).

To ease the presentation, define the aggregated constant

$$K \stackrel{\triangle}{=} \frac{F^2 dC^-}{\kappa_e RT}\left(1 - C^-\Delta V\right) \ .$$

Performing Laplace transform for the time variable of $\rho(x,z,t)$, (noting the independence of ρ in y-coordinate), one converts (3) into the Laplace domain:

$$s\rho(x,z,s) - d\frac{\partial^2 \rho(x,z,s)}{\partial x^2} + K\rho(x,z,s) = 0 \ , \tag{6}$$

where s is the Laplace variable. Define $\beta(s)$ such that $\beta^2(s) = \frac{s+K}{d}$. With an assumption of symmetric charge distribution about $x = 0$, the generic solutions can be obtained as

$$\rho(x,z,s) = 2c_2(z,s)\sinh(\beta(s)x) \ , \tag{7}$$

$$E(x,z,s) = 2c_2(z,s)\frac{\cosh(\beta(s)x)}{\kappa_e \beta(s)} + a_1(z,s) \ , \tag{8}$$

$$\phi(x,z,s) = -2c_2(z,s)\frac{\sinh(\beta(s)x)}{\kappa_e \beta^2(s)} - a_1(z,s)x + a_2(z,s) \ , \tag{9}$$

where $c_2(z,s)$, $a_1(z,s)$ and $a_2(z,s)$ depend on the boundary condition of the PDE, which will be discussed shortly.

The effect of distributed surface resistance is incorporated into the model, as illustrated in Fig. 3. Let the electrode resistance per unit length be r_1 in z direction and r_2 in x direction. R_p denotes the through-polymer resistance per

unit length. In Fig. 3, $i_p(z,s)$ is the distributed current going through the polymer due to the ion movement, $i_k(z,s)$ represents the leaking current of the polymer, and $i_s(z,s)$ is the surface current on the electrodes. Note that r_1, r_2 and R_p can be further expressed in terms of dimensions and fundamental properties of the IPMC.

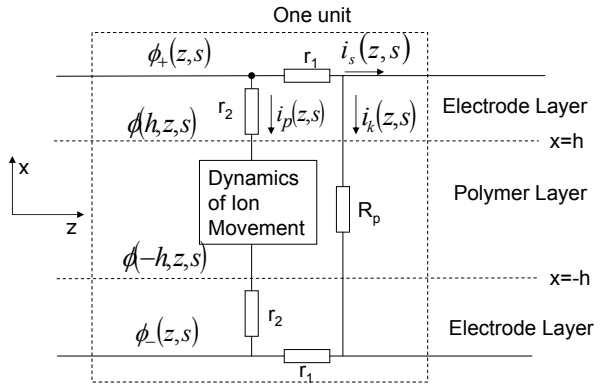

Fig. 3. Illustration of the distributed surface resistance for the IPMC impedance model.

The following equations capture the relationships between $i_s(z,s)$, $i_p(z,s)$, $i_k(z,s)$, $\phi_+(z,s)$ and $\phi_-(z,s)$:

$$\frac{\partial \phi_\pm(z,s)}{\partial z} = \mp \quad r_1 i_s(z,s) \ , \tag{10}$$

$$-\frac{\partial i_s(z,s)}{\partial z} = \quad i_p(z,s)+i_k(z,s) \ . \tag{11}$$

From the potential condition at $z=0$, i.e., $\phi_+(0,s)=\frac{V(s)}{2}$ and $\phi_-(0,s)=-\frac{V(s)}{2}$, the boundary conditions for the potential $\phi(x,z,s)$ are derived as:

$$\phi(\pm h,z,s) = \pm\frac{V(s)}{2} \mp \int_0^z r_1 i_s(\tau,s)\,d\tau \mp i_p(z,s)\,r_2 \ . \tag{12}$$

With (5) and (12) , one can solve for the functions $a_1(z,s)$ and $a_2(z,s)$ $c_2(z,s)$ in the generic expressions for $\phi(x,z,s)$, $E(x,z,s)$.

Denote $\gamma(s)=\beta(s)h$. The transfer function of the impedance can be finally derived (through yet another Laplace transform on the z-variable):

$$Z_1(s) = \frac{V(s)}{I(s)} = \frac{2\sqrt{B(s)}}{A(s)\tanh\left(\sqrt{B(s)}L\right)} \ , \tag{13}$$

where

$$\theta(s) = \frac{Wk_e\gamma(s)(s+K)}{h(s\gamma(s)+K\tanh(\gamma(s)))} \ , \tag{14}$$

$$A(s) = \frac{\theta(s)}{(1+r_2\theta(s))}+\frac{2}{R_p} \ , \tag{15}$$

$$B(s) = r_1 A(s) \ . \tag{16}$$

Detailed derivation is omitted due to the space limitation. The impedance model $Z_2(s)$ ignoring surface resistance can be obtained from $Z_1(s)$ by taking $r_1\to 0$, $r_2\to 0$ and $R_p\to\infty$:

$$Z_2(s) = \frac{s+K\frac{\tanh(\gamma(s))}{\gamma(s)}}{Cs(s+K)} \ . \tag{17}$$

IV. MODEL OF ACTUATION RESPONSE

Based on the impedance model, one can derive the actuation model by assuming the coupling between the charge density and the induced stress as in (4). However, the dynamics of cantilevered beam will also affect the actuation behavior when the excitation frequency is close to the natural frequency of the beam. The actuation model is thus a cascade of two modules, the electrodynamic $H(s)$ and the viscoelastic beam dynamics $G(s)$, as shown in Fig 4.

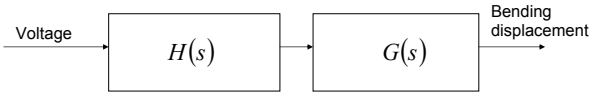

Fig. 4. Actuation model structure.

We define the moment profile in z direction as

$$M(z,s) = \int_{-h}^{h} x\sigma(x,z,s)\,W dx = \int_{-h}^{h} x\alpha_0\rho(x,z,s)\,W dx \ . \tag{18}$$

Following the static cantilevered beam theory [11], with $M(z,s)$, one can develop the transfer function relating the bending displacement to the actuation voltage:

$$H(s) = \frac{\alpha_0 W}{YI}\frac{Kk_e(\gamma(s)-\tanh(\gamma(s)))}{(\gamma(s)s+K\tanh(\gamma(s)))}\left(\frac{X(s)}{1+r_2\theta(s)}\right) \ , \tag{19}$$

where

$$X(s) = \frac{1-\operatorname{sech}\left(\sqrt{B(s)}L\right)-\tanh\left(\sqrt{B(s)}L\right)\sqrt{B(s)}L}{B(s)} \ , \tag{20}$$

Y is the static Young's modulus of the IPMC, and $I=\frac{2}{3}Wh^3$ is the moment of inertia of the IPMC.

The dynamics of the viscoelastic beam $G(s)$ with small deflection can be described by a second-order system:

$$G(s) = \frac{\omega_n^2}{s^2+2\xi\omega_n+\omega_n^2} \ , \tag{21}$$

where ω_n is the natural frequency of the IPMC cantilever beam, ξ is the damping ratio. The natural frequency ω_n can be further expressed in terms of the beam dimensions and mechanical properties [12].

V. MODEL REDUCTION

An important motivation for deriving a transfer function-type actuation model is its potential use for real-time feedback control. For practical implementation of feedback control design, the model needs to be finite-dimensional, i.e., being a finite-order, rational function of s.

For ease of presentation, decompose $H(s)$ as

$$H(s) = f(s)\cdot g(s)\cdot X(s) \ , \quad \text{where}$$

$$f(s) = \frac{L^2\alpha_0 W}{2YI}\frac{K\kappa_e(\gamma(s)-\tanh(\gamma(s)))}{(\gamma(s)s+K\tanh(\gamma(s)))} \ , \tag{22}$$

$$g(s) = \frac{2}{1+r_2\theta(s)/W} \ . \tag{23}$$

Based on the physical parameters (see Table I in Section VI), for operating frequencies within typical IPMC actuation bandwidth (< 100Hz),

$$\tanh(\gamma(s)) \approx 1 , \tag{24}$$

$$\gamma(s) \approx h\sqrt{\frac{K}{d}} =: \gamma . \tag{25}$$

Then one can simplify $f(s)$ and $g(s)$ as

$$f(s) \approx -\frac{L^2\alpha_0 W}{2YI}\frac{K\kappa_e(\gamma-1))}{(\gamma s+K)} . \tag{26}$$

$$\theta(s) \approx \frac{sW\kappa_e\gamma(s+K)}{h(\gamma s+K)} , \tag{27}$$

$$g(s) \approx \frac{2h(\gamma s+K)}{r_2\gamma\kappa_e s(s+K)+h(\gamma s+K)}. \tag{28}$$

Through Taylor series expansions of $\sinh(a)$ and $\cosh(a)$, one can approximate $X(s)$ by:

$$X(s) \approx \frac{1+\sum_{n=0}^{m}\left(\frac{a^{2n+2}}{(2n+1)!}-\frac{a^{2n}}{(2n)!}\right)}{\sum_{n=0}^{m}\frac{a^{2n+2}}{(2n)!}} , \tag{29}$$

where $a=\sqrt{B(s)}L$, for some finite integer m. Combining (26), (28), and the approximation to $X(s)$, one gets a rational approximation to $H(s)$.

VI. EXPERIMENTAL VERIFICATION

A. Experimental setup

Fig. 5 shows the experimental setup. The IPMC materials used in this work were obtained from Environmental Robots Inc. An IPMC sample is dipped in water and clamped at one end. The IPMC is subject to voltage excitation generated from the computer (through dSPACE DS1104 and ControlDesk). A laser displacement sensor is used to measure the bending displacement $w(t)$. A current-amplifier circuit is used to measure the IPMC actuation current.

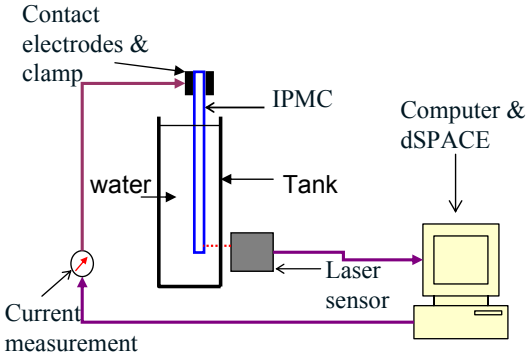

Fig. 5. Experimental setup.

B. Parameter Identification

In the dynamic impedance models $Z_1(s)$ and $Z_2(s)$, some parameters are physical constants (gas constant R and Faraday's constant F), some can be measured directly (absolute temperature T, static Young's modulus Y, actuator dimensions, surface resistance r_1 in z direction and resistance of the polymer R_p), and the others need to be identified through curve-fitting. Table I lists all the constants and identified parameters. Since $|C^-\Delta V| \ll 1$ [7], we take $1-C^-\Delta V = 1$.

TABLE I

PARAMETERS IN THE MODEL.

F	R	T	R_p
96487 C/mol	8.3143 J/mol · K	300 K	67 Ω·m
Y [4]	h	r_1	r_2
5.71×10^8 Pa	180 (μm)	4363 Ω/m	8.2^{-3} Ω· m
d	C^-	κ_e	α_0
3.39×10^{-7} m^2/s	1091 mol/m^3	1.48×10^{-6} F/m	0.1 J/C
r_2	ω_n	ξ	
8.2^{-3} Ω· m	33.6 rad/sec	0.125	

C. Impedance Model Verification

Impedance model verification will be conducted on two aspects. First, it will be shown that the model considering the surface resistance is more accurate than the model ignoring the resistance, by comparing them with the measured frequency response of an IPMC actuator. Second, the geometric scalability of the proposed model will be confirmed by the agreement between model predictions and experimental results for IPMC actuators with different dimensions.

1) Effect of surface resistance.: In order to examine the difference between the impedance models $Z_1(s)$ and $Z_2(s)$, their model parameters were identified separately through the nonlinear fitting process. The experimental data were obtained for an IPMC actuator with dimensions $37\times5.5\times0.36$ mm. Fig. 6 compares the predicted frequency response (both magnitude and phase) by each model with the measured frequency response, and it is clear that the model incorporating surface resistance is much more accurate.

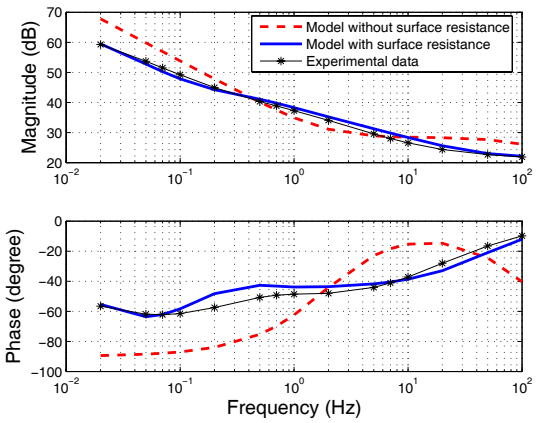

Fig. 6. Performance of the impedance models with and without consideration of surface resistance.

2) Geometric scalability of the dynamic model.: Three samples with different dimensions (see Table II) were cut from one IPMC sheet, and were labeled as *Big*, *Slim*, and *Short* for ease of referencing. Fig. 7 and Fig. 8 show the Bode plots of the impedance responses for different samples. It can be seen that for all samples, good agreement between the model prediction and the experimental data is achieved. The figures also indicate that the model is geometrically scalable.

TABLE II

DIMENSIONS OF THREE IPMC SAMPLES USED FOR VERIFICATION OF MODEL SCALABILITY.

IPMC beam	length (mm)	width (mm)	thickness (μm)
Big	39	11	360
Slim	37	5.5	360
Short	27	5.5	360

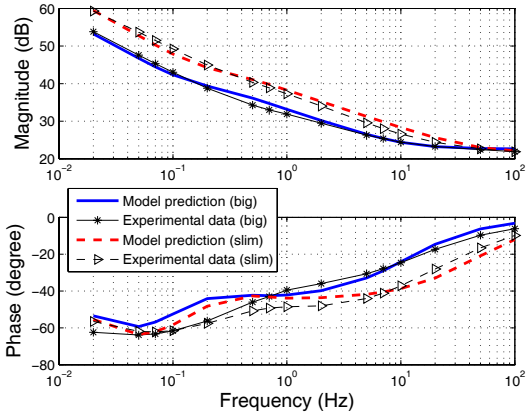

Fig. 7. Impedance of the IPMC for the *Big* and *Slim* samples.

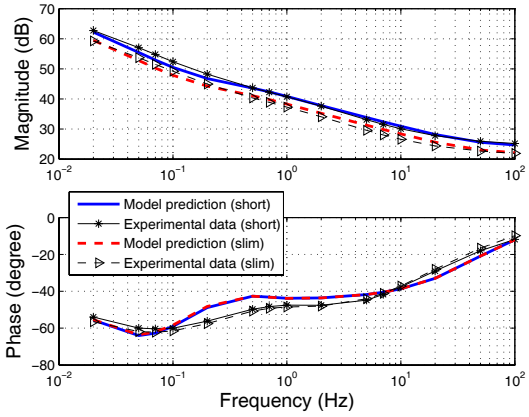

Fig. 8. Impedance of the IPMC for the *Slim* and *Short* Samples.

D. Verification of actuation model

The whole actuation model is verified in the experiment by applying sinusoid voltage signal $V(t)$ with amplitude 0.2 V and frequency from 0.02 Hz to 20 Hz. Note that since nonlinearities in IPMC actuation are not considered here, only small actuation voltages are applied to the IPMC in order to verify the proposed linear model. From Fig. 9, the simulation data based on the actuation model $G(s)\cdot H(s)$ match the experimental data well.

Model reduction was then carried out for $H(s)$ using the techniques discussed in Section V, where $m=2$ was used. It leads to a fourth-order model for the overall actuation response for the *Big* sample:

$$P(s)=\hat{H}(s)\cdot G(s)=\frac{0.0046s+0.038}{s^2+73.2s+186}\cdot\frac{835}{s^2+5.2s+835}. \quad (30)$$

From Fig. 9, the reduced model also matches closely the empirical response. It will be used for model-based controller design in the next section.

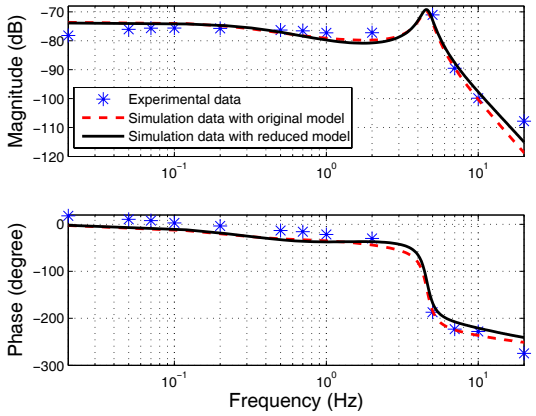

Fig. 9. Bode plot of the actuation model for *Big* sample.

VII. CONTROLLER-DESIGN EXAMPLE: MODEL-BASED H_∞ CONTROL

In this section we provide an example to illustrate the use of the proposed model in model-based controller design. While other control design methodologies can be adopted, H_∞ control has been chosen to accommodate multiple considerations, including attenuation of the effect of sensing noise, and minimization of control effort.

Consider Fig. 10, where the IPMC is represented by a nominal model $P(s)$ (30) with an additive uncertainty Δ_a. The signals d_1 and d_2 denote the actuation noise and the sensing noise, respectively. $W_e(s)$ and $W_u(s)$ are the performance weight and control weight, respectively. Standard H_∞ control techniques [13] are used in the controller design.

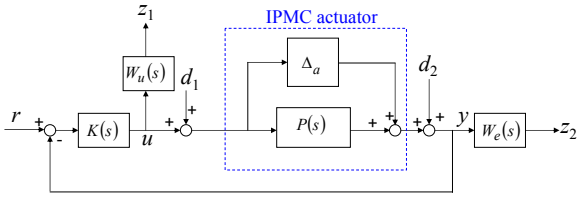

Fig. 10. Schematic of the closed-loop control system for an IPMC actuator.

The laser sensor for measuring the tip displacement has a noise level of ± 0.02 mm. For comparison purposes, a PI controller was also implemented together with a low-pass filter for the output measurement. Fig. 11 and Fig. 12 show the IPMC tracking performance under model-based H_∞ control and PI control, respectively. It can be seen that the tracking error under H_∞ control is almost at the level of sensing noise, while the error under PI control is about twice as large. Fig. 13 further compares the controller output under H_∞ control and PI control, which shows that the H_∞ control requires lower control effort. Therefore, controller design based on the reduced model is effective.

VIII. CONCLUSIONS AND FUTURE WORK

In this paper a dynamic model for IPMC actuators was developed by solving the physics-governing PDE analytically in the Laplace domain. It is distinguished from existing modeling work of IPMC actuators in that it is amenable to model

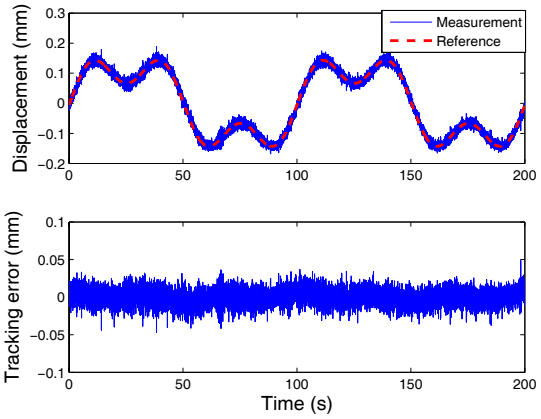

Fig. 11. Experimental results on tracking of IPMC actuator under H_∞ control.

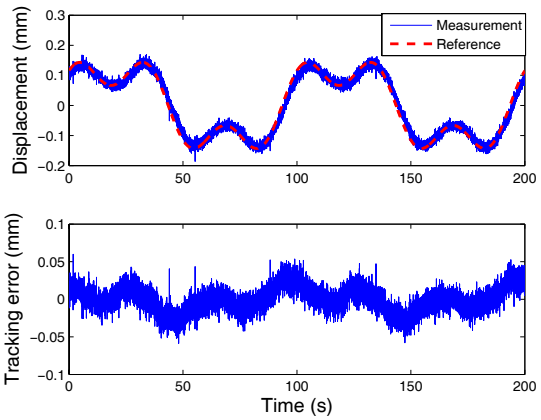

Fig. 12. Experimental results on tracking of IPMC actuator under PI control.

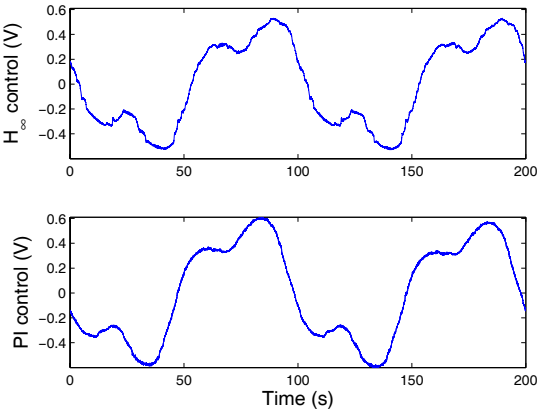

Fig. 13. Comparison of controller outputs under H_∞ control and PI control.

reduction and control design while capturing fundamental physics. The model also incorporates the effect of surface electrode resistance in an integrative manner. The compact, explicit, transfer-function representation of the physics-based model can be reduced to low-order models for real-time feedback control purposes. A number of experimental results were presented to demonstrate the geometric scalability of the model. An H_∞ controller based on the reduced low-order model has been designed and implemented in real-time tracking experiments. Experimental results have proven that the proposed model is faithful and suitable for control design.

Future work will be focused on two aspects. First, the proposed actuation model will be extended to incorporate material nonlinearities which become pronounced at large actuation levels. The nonlinearities include nonlinear elasticity, hysteresis [14], asymmetric charge distribution [10] and the dependence of parameters (such as surface resistance) on the curvature output [15].

The second direction of future work is the application of the proposed modeling approach to control of micromanipulation [4] and biomimetic robots [3]. There the model has to be extended to account for force interactions with external objects.

IX. ACKNOWLEDGMENTS

This research was supported in part by an NSF CAREER grant (ECS 0547131), MSU IRGP (05-IRGP-418), and a Summer Dissertation Fellowship awarded to Z. Chen by the MSU Graduate School and by Microsoft Inc.

REFERENCES

[1] M. Shahinpoor and K. Kim, "Ionic polymer-metal composites: I. Fundamentals," *Smart Materials and Structures*, vol. 10, pp. 819–833, 2001.

[2] K. J. Kim and M. Shahinpoor, "Ionic polymer-metal composites: II. manufaturing techniques," *Smart Materials and Structures*, vol. 12, pp. 65–79, 2003.

[3] X. Tan, D. Kim, N. Usher, D. Laboy, J.Jackson, A.Kapetanovic, J. Rapai, B. Sabadus, and X. Zhou, "An autonomous robotic fish for mobile sensing," in *Proceedings of the IEEE/RSJ International Conference on Intelligent Robots and Systems*, Beijing, China, 2006, pp. 5424–5429.

[4] Z. Chen, Y. Shen, N. Xi, and X. Tan, "Integrated sensing for ionic polymer-metal composite actuators using PVDF thin films," *Smart Materials and Structures*, vol. 16, pp. S262–S271, 2007.

[5] R. Kanno, A. Kurata, S. Tadokoro, T. Takamori, and K. Oguro, "Characteristics and modeling of ICPF actuator," *Proceedings of the Japan-USA Symposium on Flexible Automation*, pp. 219–225, 1994.

[6] K. M. Newbury and D. J. Leo, "Linear electromechanical model for ionic polymer transducers - part I: model development," *Journal of Intelligent Material Systems and Structures*, vol. 14, pp. 333–342, 2003.

[7] S. Nemat-Nasser and J. Li, "Electromechanical response of ionic polymer-metal composites," *Journal of Applied Physics*, vol. 87, no. 7, pp. 3321–3331, 2000.

[8] K. M. Farinholt, "Modeling and characterization of ionic polymer transducers for sensing and actuation," Ph.D. dissertation, Virginia Polytechnic Institute and State University, 2005.

[9] M. Shahinpoor and K. J. Kim, "The effect of surface-electrode resistance on the performance of ionic polymer-metal composite (IPMC) artificial muscles," *Smart Materials and Structures*, vol. 9, pp. 543–551, 2000.

[10] S. Nemat-Nasser, "Micromechanics of actuation of ionic polymer-metal composites," *Journal of Applied Physics*, vol. 92, no. 5, pp. 2899–2915, 2002.

[11] J. M. Gere and S. Timoshenko, *Mechanics of Materials*, 4th ed. Boston, MA: PWS Publishing Company, 1997.

[12] E. Voltera and E. C. Zachmanoglou, *Dynamics of Vibration*. Charles E. Merrill Books, Inc., 1965.

[13] K. Zhou, *Essentials of Robust Control*. Upper Saddle River, New Jersey: Prentice Hall, 1998.

[14] Z. Chen, X. Tan, and M. Shahinpoor, "Quasi-static positioning of ionic polymer-metal composite (IPMC) actuators," in *Proceedings of the IEEE/ASME International Conference on Advanced Intelligent Mechatronics*, Monterey, CA, 2005, pp. 60–65.

[15] A. Punning, M. Kruusmaa, and A. Aabloo, "Surface resistance experiments with IPMC sensors and actuators," *Sensors and Actuators A*, vol. 133, pp. 200–209, 2007.